Supporting Information

Highly Efficient Electrochemical N_2 Reduction over Strongly-Coupled CeO_2-Mo_2C Nanocomposites Anchored by Reduced Graphene Oxide

Bin Fang [a,b,c,d], *Huilin Wang* [c,d], *Meng Zhao* [c,d], *Jing Xu* [c,d], *Xiao Wang* [c,d *], *Shuyan Song* [c,d *], *and Hongjie Zhang* [c,d,e*]

[a] School of Rare Earths, University of Science and Technology of China, Hefei 230026, China

[b] Ganjiang Innovation Academy, Chinese Academy of Sciences, Ganzhou 341000, China

[c] State Key Laboratory of Rare Earth Resource Utilization, Changchun Institute of Applied Chemistry, Chinese Academy of Sciences, Changchun 130022, China

[d] School of Applied Chemistry and Engineering, University of Science and Technology of China, Hefei 230026, China

[e] Department of Chemistry, Tsinghua University, Beijing 100084, China

*Email: wangxiao@ciac.ac.cn; songsy@ciac.ac.cn; hongjie@ciac.ac.cn

Experimental Section

Chemicals.

Ammonium molybdate [$(NH_4)_6Mo_7O_{24}\cdot 4H_2O$] and Cerium nitrate hexahydrate [$Ce(NO_3)_3\cdot 6H_2O$] were purchased from Aladdin Chemical Co. Ltd. Sodium sulfate (Na_2SO_4) was purchased from Sinopharm Chemical Reagent Co., Ltd. Hydrogen peroxide solution (H_2O_2, 30wt% in H_2O) was acquired from XiLong Scientfic Co., Ltd. Graphene oxide (GO) was purchased from Shenzhen Suiheng Technology Co., Ltd. Ethyl alcohol (C_2H_5OH) was acquired from Tianjin Fuyu Fine Chemical Co., Ltd. Hydrazine monohydrate ($N_2H_4\cdot H_2O$, ≥50%) obtained from Beijing Yili Fine Chemicals Co., Ltd. Salicylic acid ($C_7H_6O_3$), sodium citrate dehydrate ($C_6H_5Na_3O_7\cdot 2H_2O$), sodium hydroxide (NaOH), hypochlorite solution (NaClO, 6-14%), sodium nitroferricyanidedihydrate ($C_5FeN_6Na_2O\cdot 2H_2O$), p-dimethylaminobenzaldehyde ($C_9H_{11}NO$) and ammonium chloride (NH_4Cl) obtained from Macklin. 212 Nafion membrane and nafion solution were acquired from DuPont. All chemicals were analytical grade and used without further purification.

Characterization.

The morphologies of samples were characterized by field emission scanning electron microscope (FEI, Qunta250, USA) and transmission electron microscope (FEI, TECNAI G2) accelerating voltage of 20 kV. X-ray diffraction (XRD) pattern was carried out using a Bruker D8 Focus powder X-ray diffractometer with Cu-Kα radiation (λ = 1.5418 Å). X-ray photoelectron spectroscopy (XPS) was analyzed by ESCALAB-MKII 250 photoelectron spectrometer with Kα radiation. Inductively coupled plasma optical emission spectroscopy (ICP-OES) data were obtained from a Varian Liberty 200 spectrophotometer. SHIMADZU UV-3600 spectrometer was used to measure the UV-Vis absorption spectra. All electrochemical tests were implemented using CHI 660E electrochemistry workstation (CH Instruments, Inc., Shanghai).

Synthesis of CeO_2/Mo_2C@rGO catalyst.

The CeO_2/Mo_2C@rGO was prepared by a thermal reduction treatment, in detail, GO (50 mg), $(NH_4)_6Mo_7O_{24}\cdot 4H_2O$ (25 mg, 0.02 mmol) and Ce $(NO_3)_3\cdot 6H_2O$ (0.92 mg,

0.002 mmol) were dispersed in 20 mL ethanol to generate a homogeneous suspension under constant stirring. After the above suspension was dried at 60 ℃ with constant stirring, a claybank mixture of GO, $(NH_4)_6Mo_7O_{24}\cdot 4H_2O$ and Ce $(NO_3)_3\cdot 6H_2O$ was obtained. The resultant claybank mixture was then annealed at 800 ℃ for 3 h under an N_2 atmosphere. After cooling to room temperature, the product of CeO_2/Mo_2C@rGO was obtained. To investigate the effect of the doped Ce, the CeO_2/Mo_2C@rGO-L and CeO_2/Mo_2C@rGO-H were also synthesized using the same procedure as above by controlling with the amounts of Ce $(NO_3)_3\cdot 6H_2O$ (0.46 mg and 1.84 mg).

Synthesis of Mo_2C@rGO catalyst.

The synthesis of Mo_2C@rGO was the same as that of above preparing CeO_2/Mo_2C@rGO, except that there was no Ce $(NO_3)_3\cdot 6H_2O$ added.

Synthesis of CeO_2@rGO catalyst

The synthesis of CeO2@rGO was the same as that of above preparing CeO_2/Mo_2C@rGO, except that there was no $(NH_4)_6Mo_7O_{24}\cdot 4H_2O$ added.

Synthesis of CeO_2 and rGO catalysts.

Ce $(NO_3)_3\cdot 6H_2O$ (20 mg) or GO (50 mg) was directly annealed using the same method as above CeO_2/Mo_2C@rGO to prepare CeO_2 and rGO catalyst, respectively.

NRR cathode preparation.

Typically, 5 mg of catalyst and 40 μL Nafion solution (DuPont, 5 wt%) were dissolved in 960 μL mixed water/ethanol solution (v/v = 1 : 1) by sonicating for 1 h to form a homogeneous ink. 20 μL of the above catalyst ink was then dropped onto a carbon paper with an area of 1 x 1 cm^2 which was next dried at 60 °C for 1 h. The loading mass of catalyst is 0.1 mg cm^{-2}.

Electrochemical measurements.

The electrocatalytic NRR was implemented in an H-type cell, which was separated by a Nafion 212 membrane. Before the NRR experiments, this Nafion 212 membrane was pretreated by H_2O_2 (5%) aqueous solution and deionized water at 80 °C for 1h, respectively. The electrocatalytic NRR measurements were carried out in a CHI 660e electrochemical workstation in a standard three-electrode system. The carbon paper

coated with catalysts used as working electrode, and an Ag/AgCl (saturated 3 M KCl electrolyte) and Pt foil were used as reference electrode and counter electrode, respectively. The potentials used in this work were translated to reversible hydrogen electrode (RHE) using the following formula: E (*vs.* RHE) =E (*vs.* Ag/AgCl) + 0.197 + 0.059 × pH. Prior to NRR tests, pure N_2 or Ar was fed into electrolyte of 0.1 M Na_2SO_4 solution (40 mL) for 0.5 h. Then chronoamperometry tests were conducted at different potentials for 1h with continuous gas feeding.

Determination of the produced ammonia.

The produced ammonia was determined by indophenol blue method[15]. In detail, 2 mL tested 0.1 M Na_2SO_4 electrolyte was mixed with 2 mL NaOH solution (1.0 M) containing salicylic acid (5 wt%) and sodium citrate (5 wt%). Then, 1 mL of 0.05 M NaClO solution and 0.2 mL of 1 wt% $C_5FeN_6Na_2O$ (sodium nitroferricyanide) solution were sequentially added into above mixture solution. After standing for 2h at room temperature, the UV-Vis absorption spectrum of resultant solution was recorded at 655nm using an UV-vis spectrophotometer. Additionally, the concentration-absorbance calibration curve was calibrated using standard ammonia chloride with various concentrations, and the fitting curve ($y = 0.3228 x + 0.0175$, R^2=0.999) shown in Figure S11.

Determination of the produced hydrazine.

The possibly produced hydrazine in the electrolyte was determined by Watt and Chrisp method[16]. First, a mixture solution of 5.99 g p-dimethylaminobenzaldehyde, 30 mL HCl and 300 mL ethanol was prepared to use as the color reagent. Typically, 5 mL of tested 0.1 M Na_2SO_4 electrolyte was mixed with 5 mL of above color reagent. After standing for 20 min at room temperature, the UV-Vis absorption spectrum of resultant solution was recorded at 455nm using an UV-vis spectrophotometer. The concentration-absorbance calibration curve was also calibrated using standard hydrazine solutions with different concentrations, and the fitting curve ($y = 0.586 x + 0.003$, R^2=0.999) shown in Figure S12.

Calculations of NH_3 yield and FE.

The NH_3 yield and Faradaic efficiency were calculated using the following equation:

$$\text{Yield rate } (NH_3) = \frac{C\,(NH3) \times V}{m\,(cat.) \times t}$$

$$\text{FE} = \frac{3 \times F \times C\,(NH3) \times V}{17 \times Q} \times 100\%$$

where $C(NH_3)$ refers to the NH_3 concentration; V represents to volume of reaction electrolyte; m(cat.) is the catalyst loading; t is the reaction time; F represents to the Faraday constant and Q is the total charge of applied electricity.

^{15}N Isotopic Labeling Experiment.

$^{15}N_2$ (Sigma-Aldrich, enrichment of 99%) was used as feed gas to perform isotopic labeling experiments. Before electrolysis, ultrapure argon (99.999%) was purged through the electrolyte of 0.1M Na_2SO_4 for 30 min to remove excess $^{14}N_2$. During the electrolysis process, $^{15}N_2$ was continuously fed into the electrolyte and electrolyzed at -0.3V *vs* RHE for 1h. After electrolysis, 10 mL reaction solution in cathodic chamber was concentrated to 1 mL at 80 ℃ and the pH was adjusted to 2. Then 30 μL of the above solution was dissolved in 600 μL dimethyl sulfoxide-D6, followed by the addition of 10 μL maleic acid solution (20 mM, internal standard), and then the above mixture was subjected to ^{1}H NMR spectroscopy measurement. $^{14}N_2$ labeling experiment and ^{1}H NMR measurement were conducted with the same method. ^{1}H NMR calibration curves for calculating the amount of NH_3 were plotted using different concentrations of $(^{14}NH_4)_2SO_4$ and $(^{15}NH_4)_2SO_4$ solution.

DFT calculations.

The density functional theory (DFT) computations were conducted by the Vienna ab-initio simulation package (VASP) using the projector augmented wave (PAW) method.[17] The exchange-correlation potential was described by the Perdew–Burke–Ernzerhof (PBE) functional within the generalized gradient approximation (GGA).[18] The energy cutoff for plane wave expansions was set to 450 eV, and the 2×2×1 Monkhorst-Pack grid k-points were selected to sample the Brillouin zone integration. The vacuum space is adopted 15 Å above the surfaces to avoid periodic interactions. The structural optimization was completed for energy and force convergence set at

1.0×10^{-4} eV and 0.02 eV $Å^{-1}$, respectively.

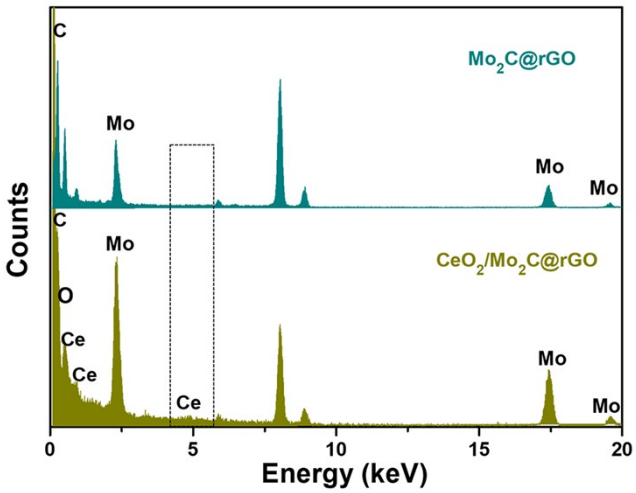

Fig. S1. EDX spectra of the as-prepared Mo_2C@rGO and CeO_2/Mo_2C@rGO.

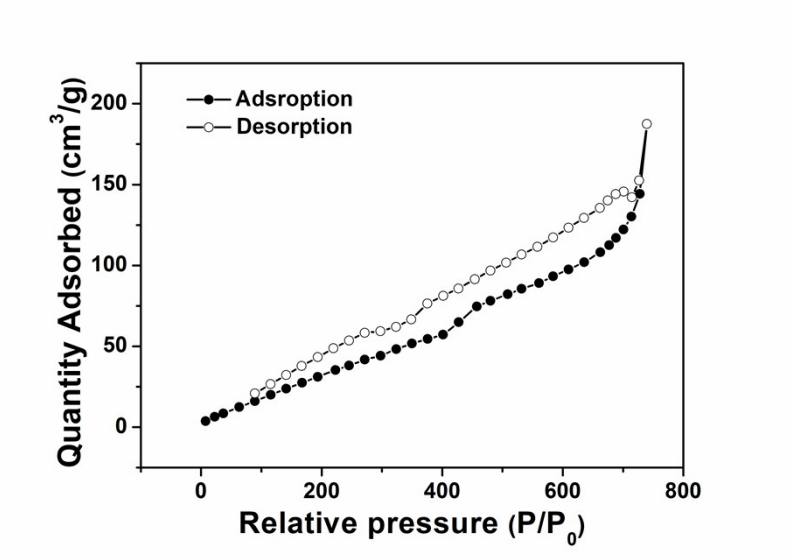

Fig. S2. Nitrogen adsorption-desorption isotherms of the as-prepared CeO_2/Mo_2C@rGO.

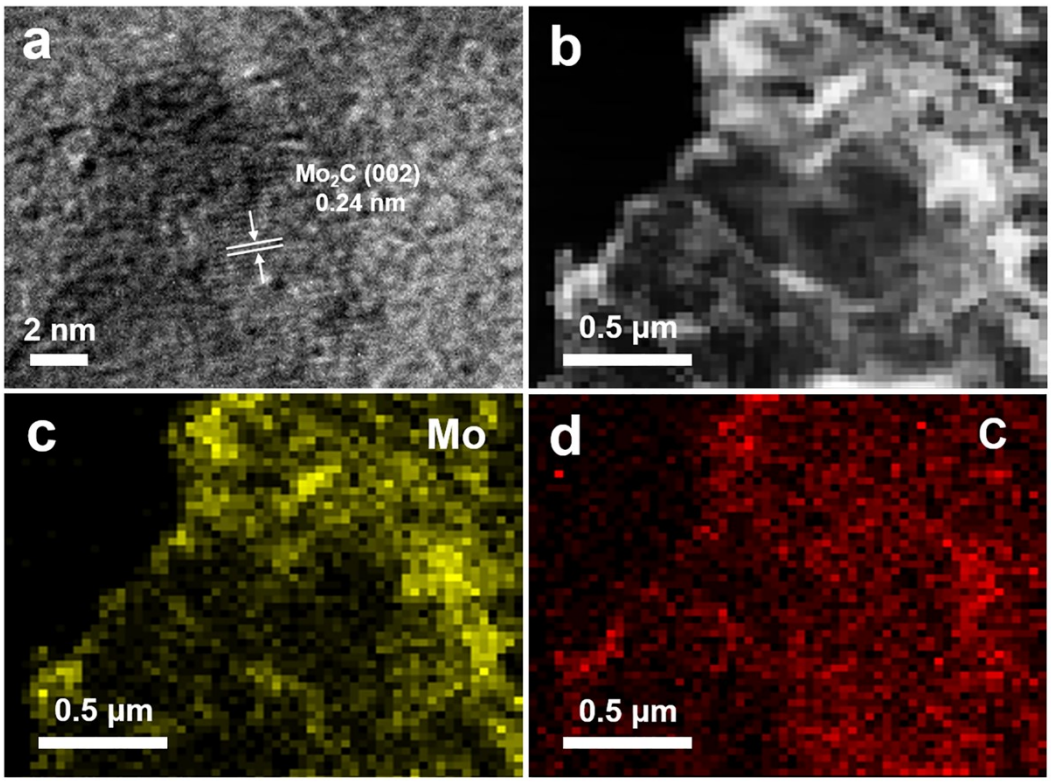

Fig. S3. (**a**) HRTEM image; (**b**) High-angle annular dark-field scanning transmission electron microscopy (HAADF-STEM) image; (**c-d**) Corresponding element mappings of the as-prepared Mo_2C@rGO.

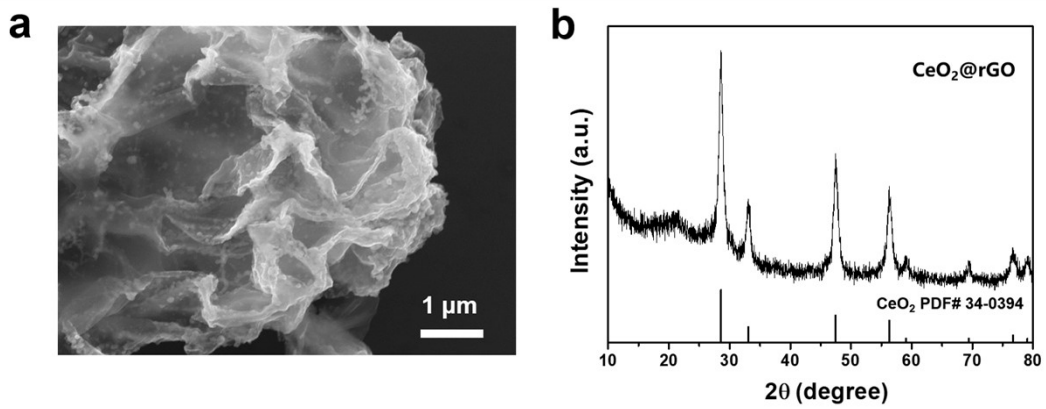

Fig. S4. (**a**) SEM image and (**b**) XRD pattern of the prepared CeO_2@rGO.

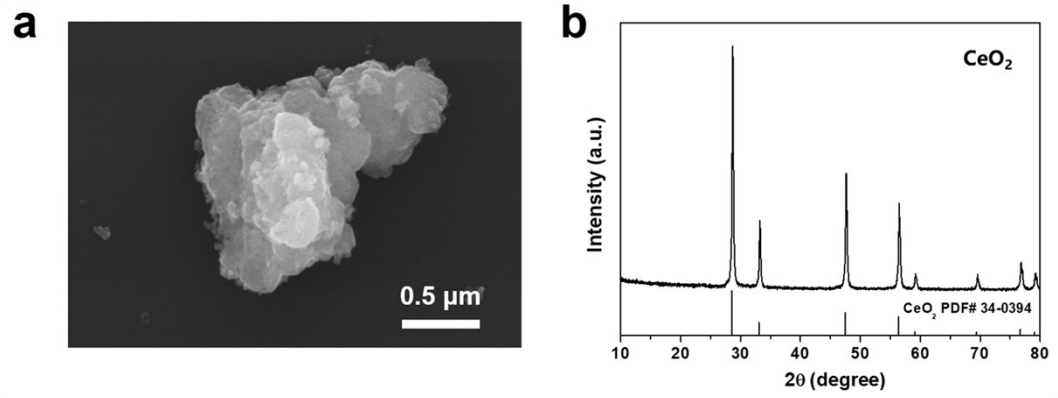

Fig. S5. (**a**) SEM image and (**b**) XRD pattern of the prepared CeO_2.

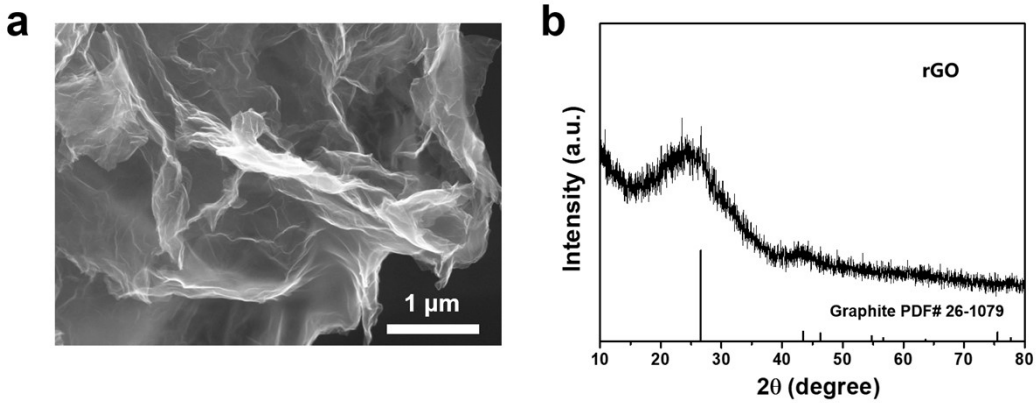

Fig. S6. (**a**) SEM image and (**b**) XRD pattern of the prepared rGO.

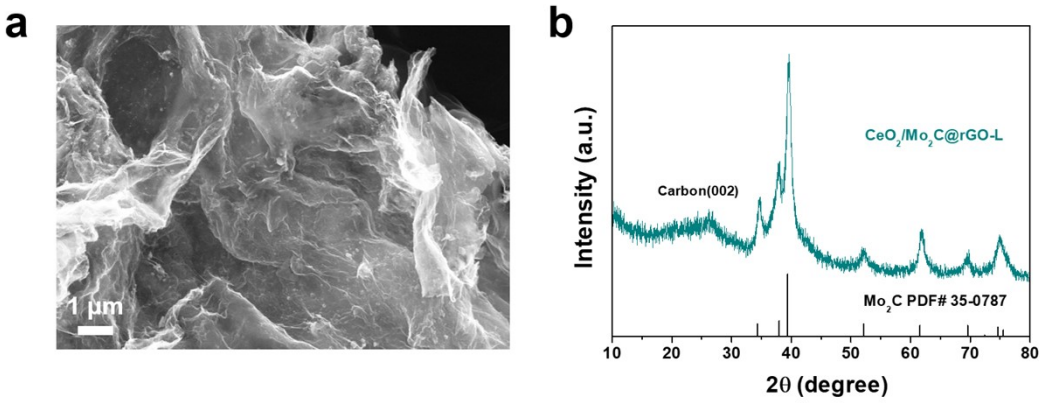

Fig. S7. (**a**) SEM image and (**b**) XRD pattern of the prepared CeO_2/Mo_2C@rGO-L.

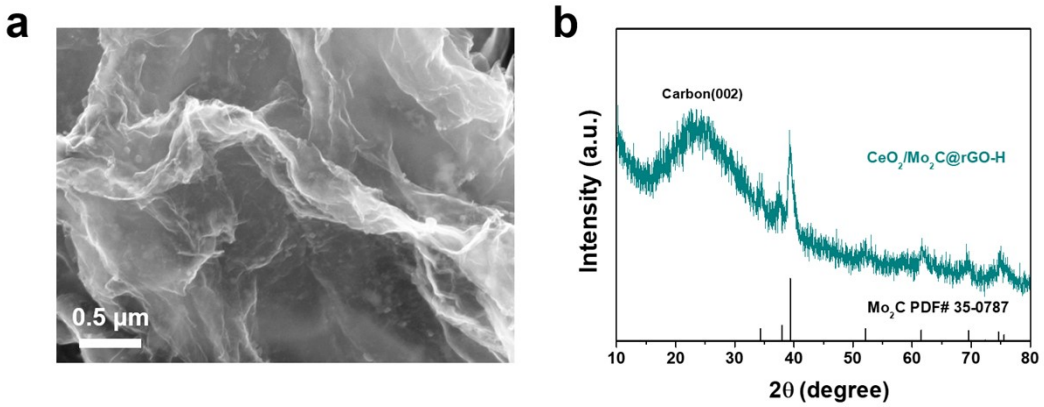

Fig. S8. (**a**) SEM image and (**b**) XRD pattern of the prepared CeO_2/Mo_2C@rGO-H.

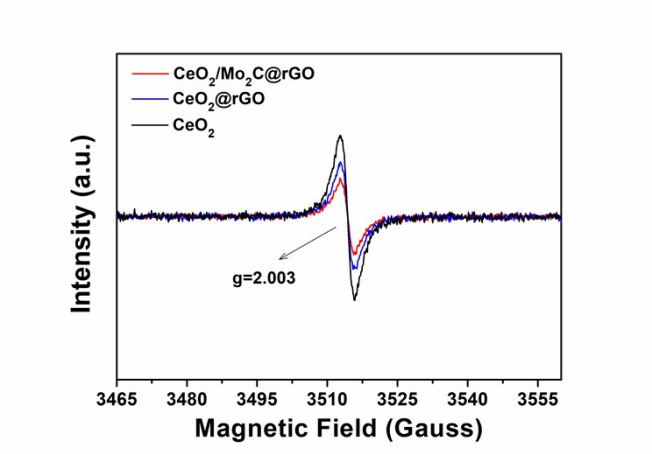

Fig. S9. EPR spectra of CeO_2/Mo_2C@rGO, CeO_2@rGO and CeO_2.

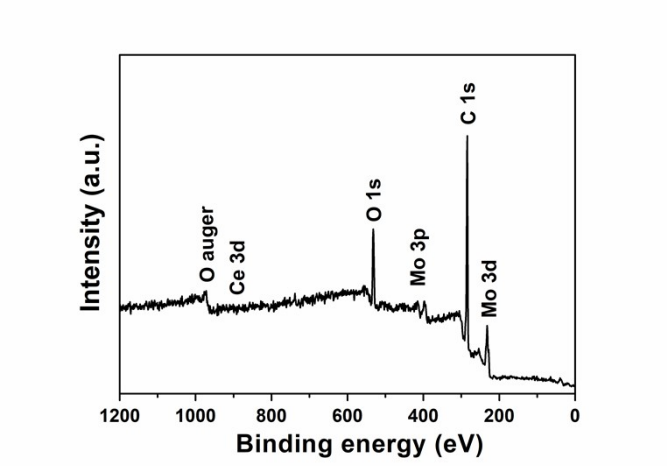

Fig. S10. XPS survey pattern of the CeO_2/Mo_2C@rGO.

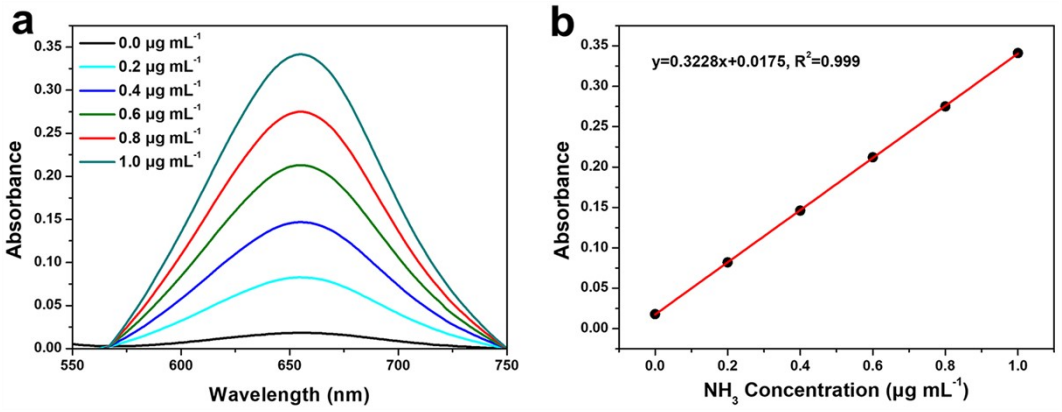

Fig. S11. (**a**) UV-Vis absorption spectra of various NH_3 concentrations after being incubated for 2 h under ambient conditions. (**b**) Calibration curve used for calculation of NH_3 concentrations.

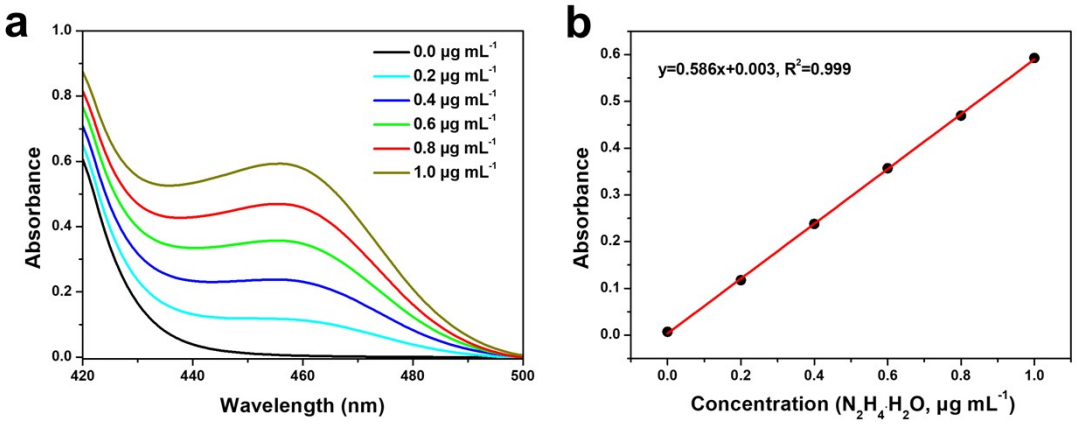

Fig. S12. (**a**) UV-Vis absorption spectra of various $N_2H_4 \cdot H_2O$ concentrations after being incubated for 10 min under ambient conditions. (**b**) Calibration curve used for calculation of $N_2H_4 \cdot H_2O$ concentrations.

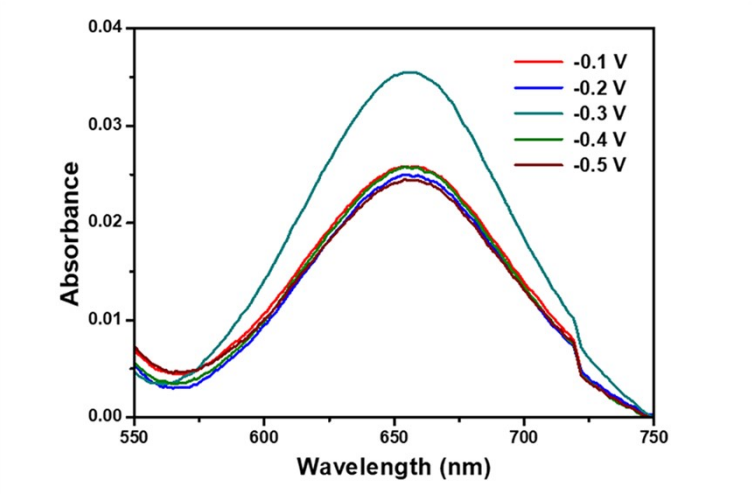

Fig. S13. UV-vis absorption spectra of the electrolytes for 10% CeO_2/Mo_2C@rGO at each given potentials.

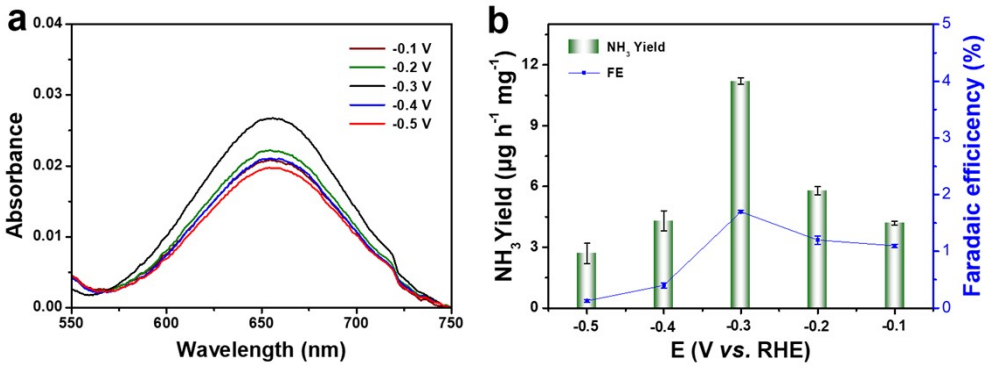

Fig. S14. (**a**) UV-vis absorption spectra of electrolyte stained with indophenol indicator at different potentials for Mo_2C@rGO. (**b**) Corresponding calculated NH_3 yield rates and Faradaic efficiencies at each given potentials.

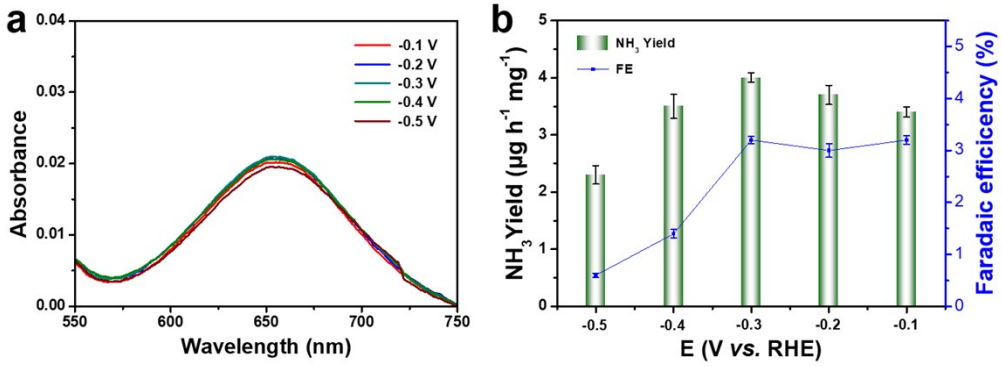

Fig. S15. (**a**) UV-vis absorption spectra of electrolyte stained with indophenol indicator for CeO_2@rGO at different potentials. (**b**) Corresponding calculated NH_3 yield rates and Faradaic efficiencies at each given potentials.

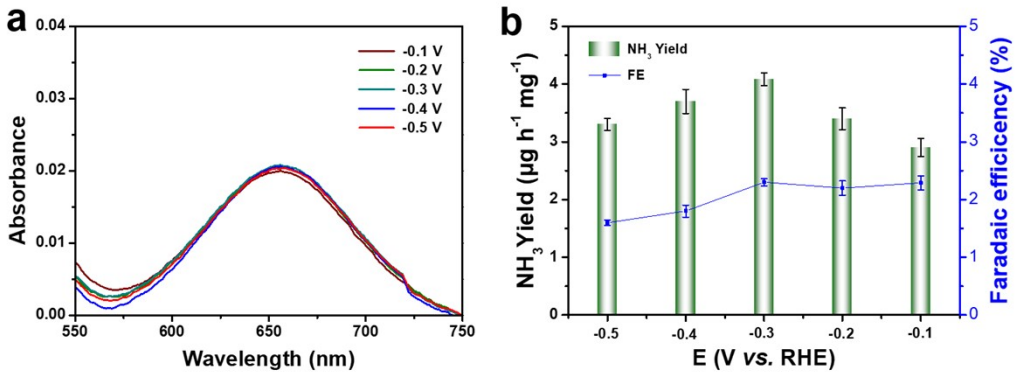

Fig. S16. (**a**) UV-vis absorption spectra of electrolyte stained with indophenol indicator for CeO_2 at different potentials. (**b**) Corresponding calculated NH_3 yield rates and Faradaic efficiencies at each given potentials.

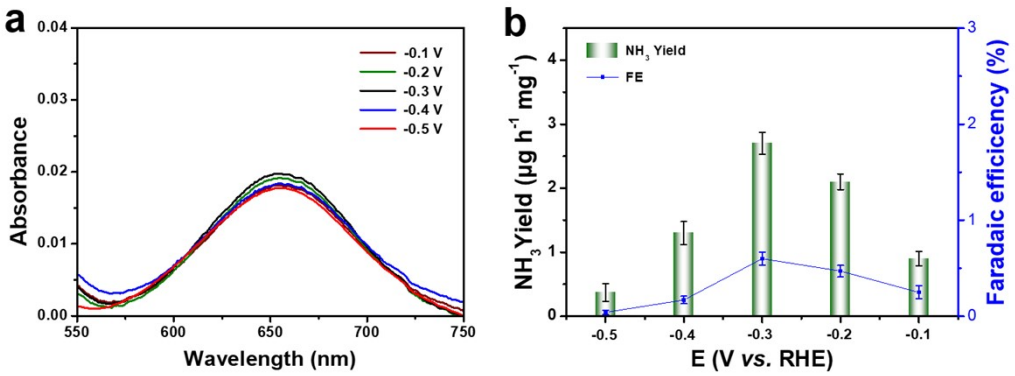

Fig. S17. (**a**) UV-vis absorption spectra of electrolyte stained with indophenol indicator for rGO at different potentials. (**b**) Corresponding calculated NH_3 yield rates and Faradaic efficiencies at each given potentials.

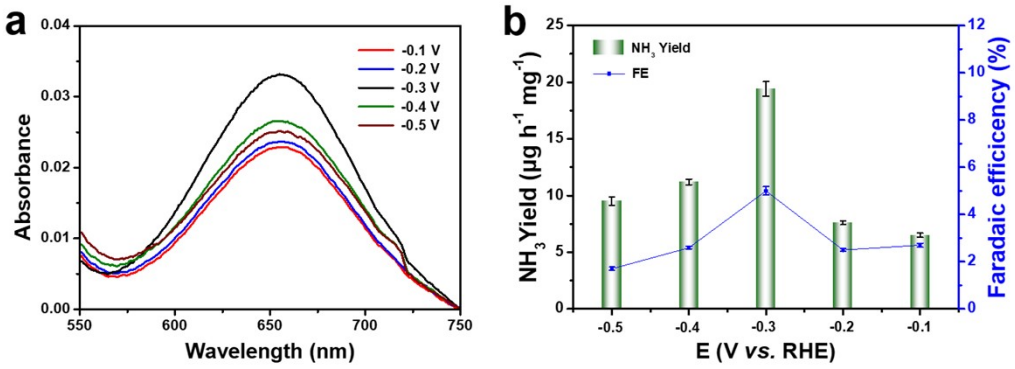

Fig. S18. (**a**) UV-vis absorption spectra of electrolyte stained with indophenol indicator for CeO_2/Mo_2C@rGO-L at different potentials. (**b**) Corresponding calculated NH_3 yield rates and Faradaic efficiencies at each given potentials.

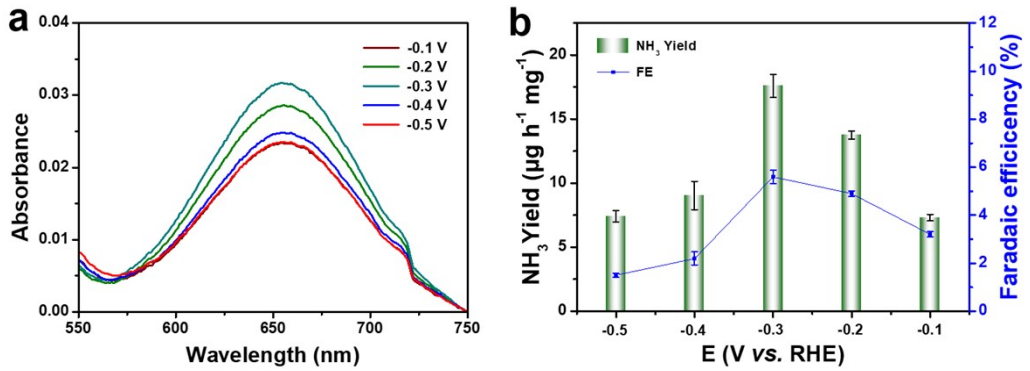

Fig. S19. (**a**) UV-vis absorption spectra of electrolyte stained with indophenol indicator for CeO_2/Mo_2C@rGO-H at different potentials. (**b**) Corresponding calculated NH_3 yield rates and Faradaic efficiencies at each given potentials.

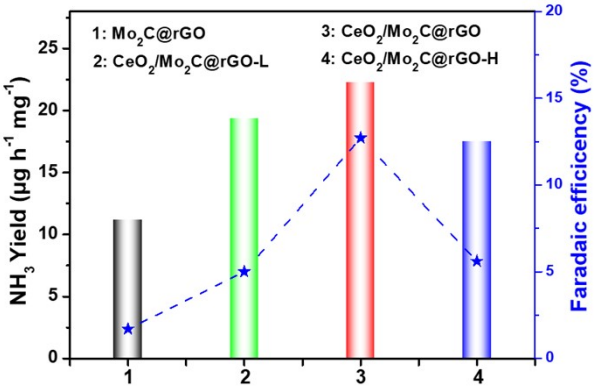

Fig. S20. The comparison of NRR performance for the CeO_2/Mo_2C@rGO doped with different concentrations of Ce.

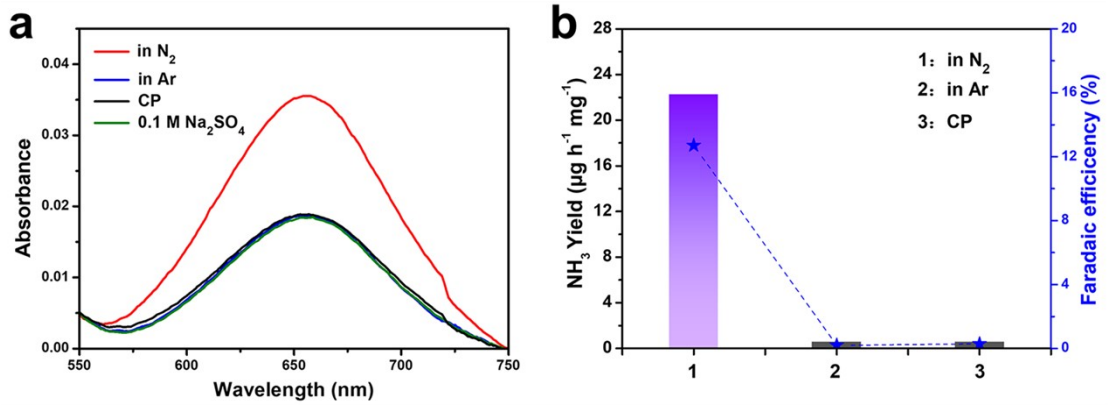

Fig. S21. (**a**) UV-vis absorption spectra of electrolyte stained with indophenol indicator for 2 h under different conditions. (**b**) Corresponding calculated NH_3 yield rates and FEs at a potential of -0.3 V for different electrodes.

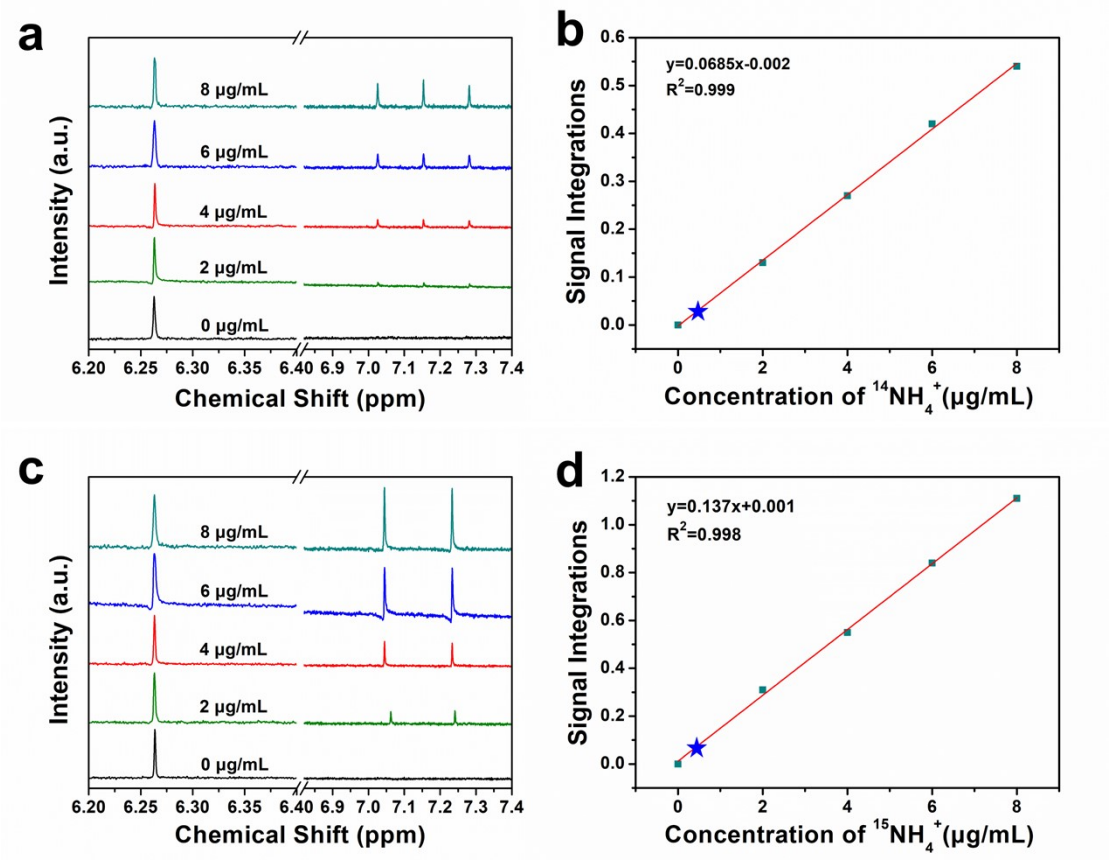

Fig. S22. (**a, b**) 1H NMR spectra of $^{14}NH_4^+$ with a series of concentrations and the corresponding calibration curve. (**c, d**) 1H NMR spectra of $^{15}NH_4^+$ with a series of concentrations and the corresponding calibration curve.

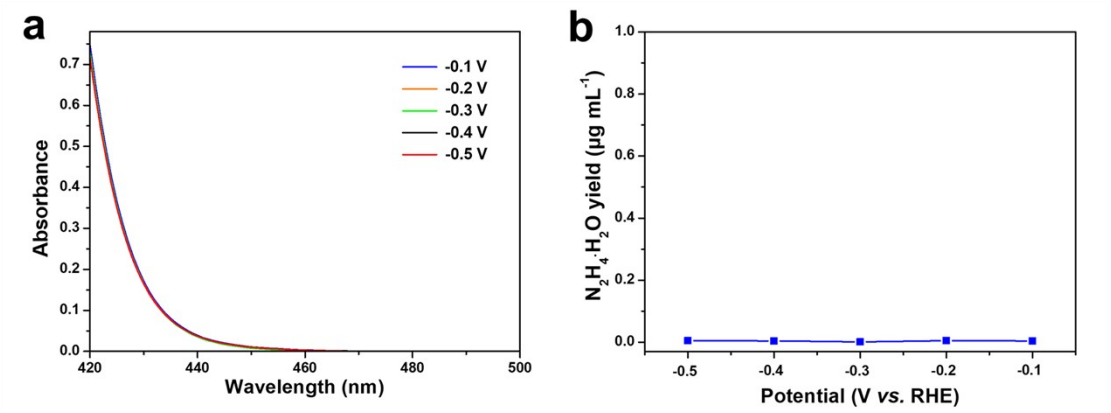

Fig. S23. (**a**) UV-Vis spectra of the electrolyte estimated by the method of Watt and Chrisp after NRR process for CeO_2/Mo_2C@rGO. (**b**) Corresponding calculated $N_2H_4 \cdot H_2O$ concentration.

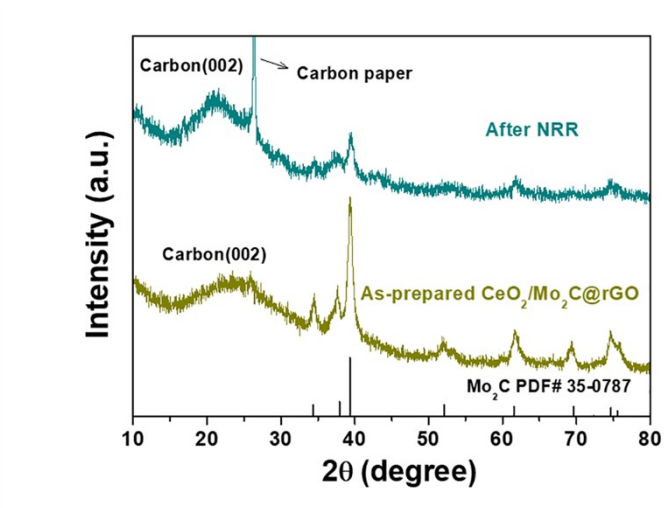

Fig. S24. XRD pattern for CeO_2/Mo_2C@rGO after 20 h stability test.

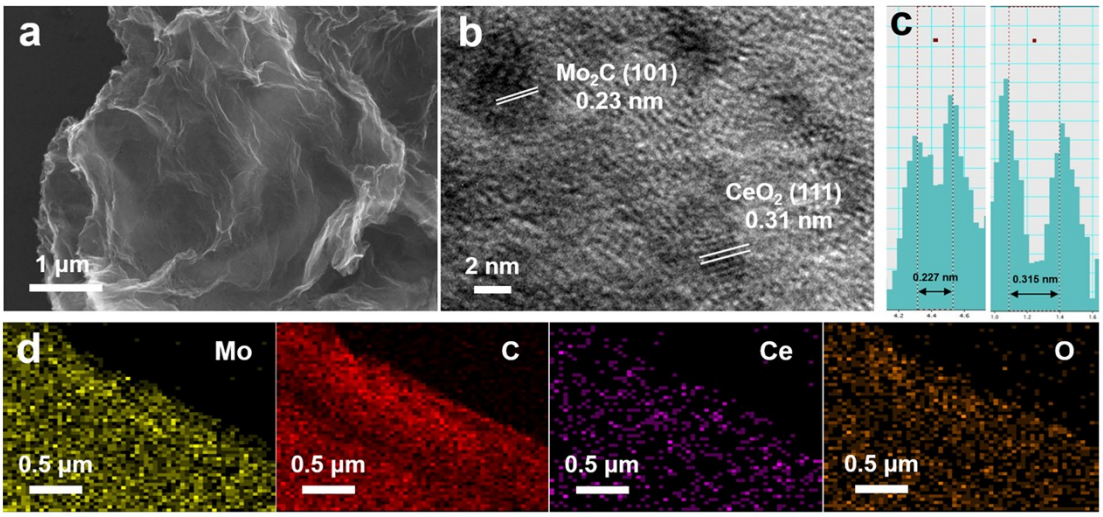

Fig. S25. Morphology of CeO_2/Mo_2C@rGO after 20 h stability test. (**a**) SEM image; (**b**) HRTEM image; (**c**) Corresponding line-scanning intensity profiles from **b**; (**d**) Elemental mapping images of CeO_2/Mo_2C@rGO after 20 h stability test.

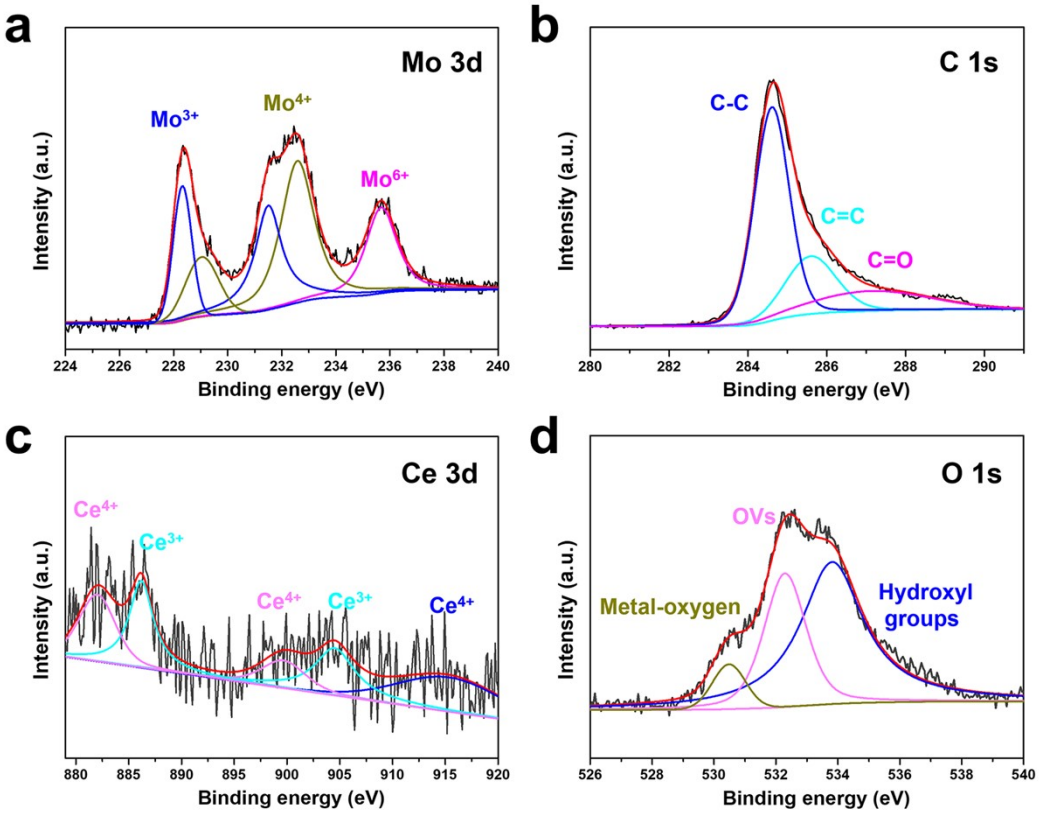

Fig. S26. XPS spectra in (**a**) Mo 3d, (**b**) C 1s, (**c**) Ce 3d and (**d**) O 1s regions of CeO_2/Mo_2C@rGO after 20 h stability test.

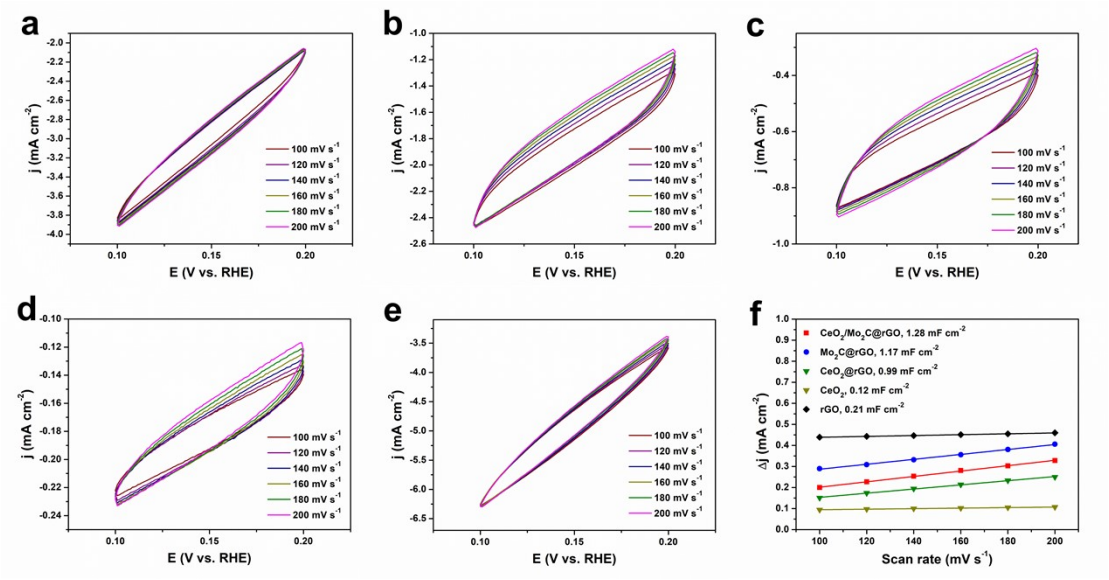

Fig. S27. CV curves of (**a**) CeO_2/Mo_2C@rGO, (**b**) Mo_2C@rGO, (**c**) CeO_2@rGO, (**d**) CeO_2 and (**e**) rGO at 100-200 mV s^{-1} in the range of 0.1 and 0.2 V *vs.* RHE. (**f**) Calculated corresponding C_{dl} values of the above samples.

Table S1. Inductively coupled plasma optical emission spectroscopy (ICP-OES) analysis of different samples.

Samples	Ce content (wt.%)
CeO_2/Mo_2C@rGO	1.1
CeO_2/Mo_2C@rGO-L	0.61
CeO_2/Mo_2C@rGO-H	2.2

Table S2. Comparison of NRR performances with reported graphene-based catalysts.

Catalyst	Electrolyte	Potential (V *vs.* RHE)	NH_3 yield ($\mu g\ h^{-1}\ mg^{-1}$)	FE (%)	Ref.
CeO_2/Mo_2C@rGO	0.1 M Na_2SO_4	-0.3	22.3	12.7	This work
IrTe 4 PNRs a-Au/CeOx-RGO	0.1 M HCl	-0.2	8.3	10.10	[1]
$Pd_{0.2}Cu_{0.8}$/rGO	0.1 M KOH	-0.2	2.8	4.5	[2]
NiO/graphene	0.1 M Na_2SO_4	-0.7	18.6	7.8	[3]
F-doped graphene	0.1 M Na_2SO_4	-0.7	9.3	4.2	[4]
O-doped graphene	0.1 M HCl	-0.55	21.3	12.6 (-0.45 V)	[5]
MoP@rGO	0.1 M Li_2SO_4	-0.6	7.5	9.1	[6]
CeO_2-rGO	0.1 M Na_2SO_4	-0.7	16.98	4.78	[7]
Fe_2O_3-rGO	0.5 M $LiClO_4$	-0.5	22.13	5.89 (-0.4 V)	[8]
ZnO@rGO	0.1 M Na_2SO_4	-0.65	17.7	6.4	[9]
mVOx@rGO	0.1 M Na_2SO_4	-0.35	18.84	16.97	[10]
In_2O_3/rGO	0.1 M Na_2SO_4	-0.7	18.4	8.1	[11]
Tannic acid-rGO	0.5 M $LiClO_4$	-0.75	17.02	4.83	[12]
N,S co-doped graphene	0.1 M HCl	-0.6	7.7	5.8	[13]
MoS_2 nanodots/rGO	0.1 M Na_2SO_4	-0.75	16.41	27.93	[14]

Supplementary references

[1] S. J. Li, D. Bao, M. M. Shi, B. R. Wulan, J. M. Yan and Q. Jiang, *Adv. Mater.*, 2017, **29**, 1700001.

[2] M. M. Shi, D. Bao, S. J. Li, B. R. Wulan, J. M. Yan and Q. Jiang, *Adv. Energy Mater.*, 2018, **8**, 1800124.

[3] K. Chu, Y. p. Liu, J. Wang and H. Zhang, *ACS Appl. Mater. Interfaces*, 2019, **2**, 2288-2295.

[4] J. Zhao, J. Yang, L. Ji, H. Wang, H. Chen, Z. Niu, Q. Liu, T. Li, G. Cui and X. Sun, *Chem. Commun.*, 2019, **55**, 4266-4269.

[5] T. Wang, L. Xia, J.-J. Yang, H. Wang, W.-H. Fang, H. Chen, D. Tang, A. M. Asiri, Y. Luo, G. Cui and X. Sun, *Chem. Commun.*, 2019, **55**, 7502-7505.

[6] Y. Zhou, X. Yu, F. Sun and J. Zhang, *Dalton Trans.*, 2020, **49**, 988-992.

[7] H. Xie, Q. Geng, X. Li, T. Wang, Y. Luo, A. A. Alshehri, K. A. Alzahrani, B. Li, Z. Wang and J. Mao, *Chem. Commun.*, 2019, **55**, 10717-10720.

[8] J. Li, X. Zhu, T. Wang, Y. Luo and X. Sun, *Inorg. Chem. Front.*, 2019, **6**, 2682-2685.

[9] Y.-p. Liu, Y.-b. Li, D. j. Huang, H. Zhang and K. Chu, *Chem-Eur J.*, 2019, **25**, 11933-11939.

[10] W. Fang, J. Zhao, T. Wu, Y. Huang, L. Yang, C. Liu, Q. Zhang, K. Huang and Q. Yan, *J. Mater. Chem. A*, 2020, **8**, 5913-5918.

[11] P. Wang, Q.-q. Li, Y.-h. Cheng and K. Chu, *J. Mater. Sci.*, 2020, **55**, 4624-4632.

[12] Y. Song, T. Wang, J. Sun, Z. Wang, Y. Luo, L. Zhang, H. Ye and X. Sun, *ACS Sustain. Chem. Eng.*, 2019, **7**, 14368-14372.

[13] Y. Tian, D. Xu, K. Chu, Z. Wei, W. Liu, *J. Mater. Sci.* 2019**, 54**, 9088-9097.

[14] Y. Liu, W. Wang, S. Zhang, W. Li, G. Wang, Y. Zhang, M. Han and H. Zhang, *ACS Sustain. Chem. Eng.*, 2020, **8**, 2320-2326.

[15] D. Zhu, L. Zhang, R. E. Ruther, R. J. Hamers, Nat. Mater., 2013, **12**, 836-841.

[16] W. C. McCrone and I. Corvin, Anal. Chem., 1952, **24**, 2008-2009.

[17] G. Kresse and J. Hafner, Phys. Rev. B, 1994, **49**, 14251-14269.

[18] P. E. Blochl, Phys. Rev. B, 1994, **50**, 17953-17979.